MULTIFIELD FALSE VACUUM DECAY: POLYGONAL BOUNCE*

Victor Guada

Jožef Stefan Institute, Jamova 39, 1000 Ljubljana, Slovenia

(Received November 18, 2019)

As in boiling super-heated liquid, first-order phase transitions in QFT arise from an abrupt decay of an excited state of false vacuum into an energetically more favorable minimum of energy through bubble nucleation. We review an efficient semi-analytical approach to compute such a tunneling decay rate with any number of scalar fields and space-time dimensions. It is based on exact analytical solutions of piece-wise linear potentials with an arbitrary number of segments that describe any given potential up to the desired precision. Contributions beyond the linear order as well as the generalization to more fields are considered and computed through analytical linear expansions within a few iterations. Thereby, this approach provides a fast and robust method for evaluating tunneling decay in theories with multiple scalar fields.

DOI:10.5506/APhysPolB.50.1859

1. Introduction

As a super-heated liquid boiling into vapor, the decay of the false vacuum is a first-order phase transition of a state of vacuum, localized in a minimum of the potential, into a more favorable lower state of energy. It is triggered by quantum and/or thermodynamic fluctuations of the fields, where the state tunnels or passes over the potential barrier. This complex phenomenon in the framework of QFT appears in different contexts of physics, from particle physics [1–4], cosmology [5–8], baryogenesis [9, 10] to condensed matter physics [11, 12], among others.

In Section 2, we introduce the main basics of the decay rate in the framework of multi-field and review a particularly closed form solution [13] that is the skeleton of our method. We develop the main ideas of polygonal bounce in Section 3, from the single to multiple fields and conclude with an outlook in Section 4.

* Presented at the XLIII International Conference of Theoretical Physics "Matter to the Deepest", Chorzów, Poland, September 1–6, 2019.

2. Vacuum decay: General formalism

We wish to consider a scalar field theory on potentials with more than one minimum as on the left of figure 1; where the state of the vacuum at the local minimum is classically stable but unbalanced due to the quantum and/or thermodynamic fluctuations of the fields. Such a decay can be derived in the WKB approximation of the Schrodinger equations, real time formalism, among other methods. One of the most known and elegant derivations is given by Coleman and Callan [3], in the Euclidean Feynman path integral in the saddle-point approximation ($\hbar \to 0$), where the amplitude of the transition is proportional to

$$Z \sim \int \mathcal{D}\varphi \, \mathrm{e}^{S_{\mathrm{E}}[\varphi]/\hbar} \, . \tag{1}$$

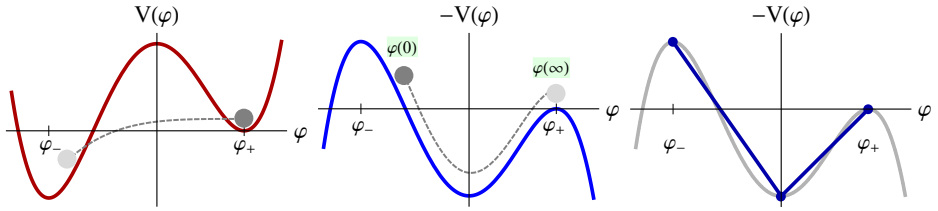

Fig. 1. (Color online) Left: An example of a potential with two minima with unstable false state of vacuum at φ_+ and a stable true one at φ_-. Center: The potential on the left after an analytic continuation into the Euclidean space. The field starts in a non-trivial value of the field φ_0 such that ends up at the true vacuum at infinity. Right: The piece-wise linear potential with two segments in black/blue circumscribed on the potential V in gray.

In this semi-classical limit, the most general expression of the decay probability per unit volume per unit time is provided by

$$\frac{\Gamma}{\mathcal{V}} = A \, \mathrm{e}^{-S_{\mathrm{E}}/\hbar} \left(1 + \mathcal{O}(\hbar)\right) \, , \tag{2}$$

where the pre-factor A depends on functional determinants and represents the loop correction of the fluctuations of the fields. This contributions are more involved and are suppressed by the exponential factor. Therefore, the main contribution dominated by the Euclidean action S_{E} for any number of space-time dimensions D and fields n_φ is

$$\mathcal{S}_{\mathrm{E}} = \int_{-\infty}^{\infty} \mathrm{d}^D x \left(\frac{1}{2} \sum_i^{n_\varphi} \nabla \varphi_i^2 + V(\varphi) \right) \, . \tag{3}$$

Note that in the transition from Minkowski to Euclidean space, there is only a minus sing difference of the potential $V_{\rm M} \to -V_{\rm E}$ or an Euclidean continuation of the time component. It was proven by [14, 15] that the solution φ is invariant under D Euclidean dimensions, for $D > 2$ and any number of fields. This implies that one can re-write and simplify action (3) by using spherical coordinates in a D-dimensional Euclidean space. Thereby, φ becomes a function of the radial coordinate $\rho = \left(\tau^2 + |\vec{x}|^2\right)^{1/2}$, and remaining $D-1$ angles are integrated out as

$$S_{\rm E} \equiv \frac{2\pi^{\frac{D}{2}}}{\Gamma\left(\frac{D}{2}\right)} \int_0^\infty \rho^{D-1} {\rm d}\rho \left(\frac{1}{2} \sum_i^{n_\varphi} \dot{\varphi_i}^2 + V \right) , \tag{4}$$

where the leading contributions are the field configurations that solve the Euler–Lagrange equations

$$\frac{{\rm d}^2\varphi_i}{{\rm d}\rho^2} + \frac{D-1}{\rho} \frac{{\rm d}\varphi_i}{{\rm d}\rho} = \frac{\partial V}{\partial \varphi_i} , \tag{5}$$

called the bounce; other possible field configurations are exponentially suppressed. This solution contains a well-defined finite energy and extremizes the action non-trivially, thereby, the boundary conditions are defined as

$$\varphi_i(0) = \varphi_0 \neq \varphi_+ , \qquad \left.\frac{{\rm d}\varphi_i}{{\rm d}\rho}\right|_0 = 0 , \qquad \lim_{\rho\to\infty} \varphi_i\left(\rho\right) = \varphi_{i,+} . \tag{6}$$

We can forget about the context that led us to derive these equations and interpret $\varphi_i(\rho)$ as the position of a particle with time ρ, (5), moving in hypersurface $-V$ and subject to a somewhat peculiar viscous damping force with a coefficient inversely proportional to time. This non-trivial term comes from the addition of extra number of space-time dimensions required in QFT, while in quantum mechanics it is simply $D = 1$. In order to satisfy the boundary conditions, the initial particle must start in a value outside the false vacuum φ_+ at time $\rho = 0$, as in the center panel of figure 1, otherwise it hits the trivial solution. Due to its damping term, if φ_0 is very far from the true vacuum ϕ_-, the particle undershoots, while if it is too close, the particle overshoots φ_+. Thereby, there is always an intermediate point that satisfies all boundary conditions, as proven by Coleman. In the analogy with the super-heated fluid, the damping term can also be understood as the energy spent in the surface tension of the bubble. Unlike quantum mechanics, this term allows phase transitions effects even without barrier.

Except for the case of quantum mechanics $D = 1$, these equations are almost impossible to solve analytically and are numerically difficult for the given boundary conditions (6). It is even more difficult for more than interacting fields, where the set of equations are coupled and the trajectory in field space (see figure 4) is curved (non-trivial). Nevertheless, for the single scalar field case, there are models where the solution can be found in closed form. One of the simplest exact solutions is the piece-wise linear potential, shown in the right panel of figure 1. The closed form bounce in $D = 4$ space-time dimensions is given by joining the solutions of each piece of the potential

$$\frac{\mathrm{d}V}{\mathrm{d}\varphi} = 8a\,\varphi + V_0\,, \qquad \varphi(\rho) = v + a\rho^2 + \frac{b}{\rho^2}\,, \tag{7}$$

where a is constant that defines the slope of the line, and b and v are constants of integration. The generalization of this simple solution to any number of segments, space-time dimension and fields is what we called the polygonal bounce [16]. This solution constituted the basic idea of our method, which finds the bounce solution for a general potential up to desired precision in a quasi-analytical form. In the next sections, we describe this simple case and progressively generalize it to multi-fields and space-time dimensions.

3. Polygonal bounce

In this section, we introduce the semi-analytical method to compute the decay rate in multi-field potentials with an arbitrary number of fields at finite and zero temperature up to desired precision, called polygonal bounce and developed in [16].

We start from the pure single field (polygonal) linear potential in Section 3.1 and compute the action for a benchmark model. We introduce second order terms in the potential through perturbative corrections in Section 3.2, where the convergence improves. In Section 3.3, we show how to compute the decay rate pre-factor that comes from loop corrections. We review the basic ideas for the multi-field potential in Section 3.4, and end with the description of the upcoming package [17] of the method in Section 3.5.

3.1. Single field polygonal bounce

Consider a piece-wise linear potential with an arbitrary number of segments circumscribed by the potential V, as shown in the top left panel of figure 2; in particular, the case of two linear pieces of the potential, *i.e.* $N = 3$ field points, and $D = 4$ was described in Section 2 and developed carefully in [13]. For any number of field points N and space-time dimensions, the solution is

$$\varphi_s(\rho) = v_s + \frac{4}{D} a_s \rho^2 + \frac{2}{D-2} \frac{b_s}{\rho^{D-2}}\,, \tag{8}$$

where a_s is a constant fixed by the potential, and v_s, b_s and R_s are constants by the boundary conditions from the matching of each segment (see [16] for more details). The potential with $N = 7$ field points (black/blue line) and its bounce solution are shown in the top left and top right panels of figure 2 respectively.

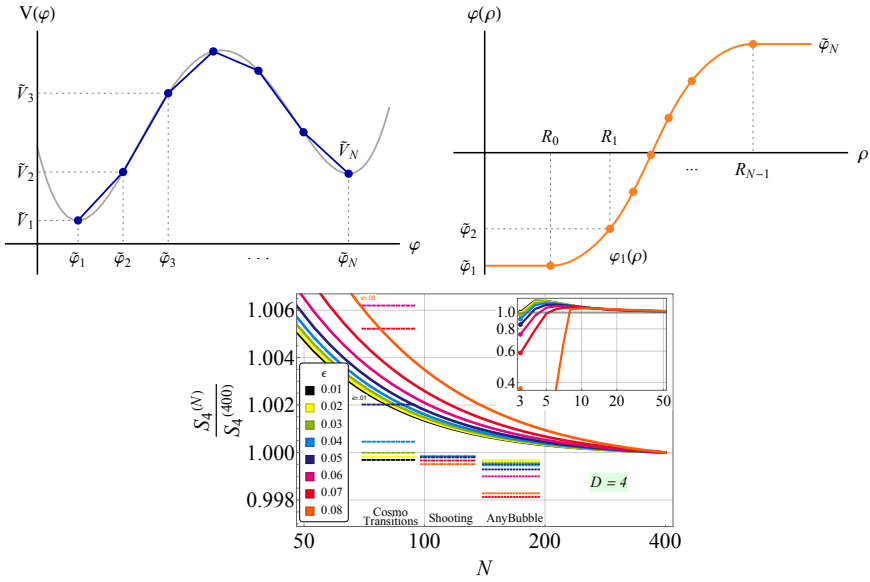

Fig. 2. (Color online) Top left: The polygonal potential with $N = 7$ field points in black/blue, circumscribed by the actual potential V in gray. Top right: The bounce field configuration of the polygonal potential on the left. Bottom: The bounce action $S_D^{(N)}$ for different values of energy gaps between the false and true vacua. It is computed with the polygonal bounce approach for different field point values N normalized to the maximal $N = 400$ uniform segmentation in $D = 4$. It is compared with other packages in the literature as CosmoTransition [18], AnyBubble [19].

The boundary conditions to obtain v, b and R come from the segmentation $\varphi(R_s) = \tilde{\varphi}_s$, continuity $\varphi_s(R_s) = \varphi_{s+1}(R_s)$, and differentiability $\dot{\varphi}_s(R_s) = \dot{\varphi}_{s+1}(R_s)$ of the bounce, which determine the complete set of coefficients and radii R of the polygonal bounce solutions. We found that these conditions can be solved analytically if and only if we solve the equation

$$a_s R_s^D - \frac{D}{4}\left(\tilde{\varphi}_{s+1} - v_s\right) R_s^{D-2} + \frac{D}{2\,(D-2)} b_s = 0 \tag{9}$$

in a closed form, which is simple for $D = 2, 3, 4, 6$ and 8 space-time dimensions. These equations are left with a single parameter that has to be computed numerically when $N > 3$. Nevertheless, since a part of the solution is known in a closed form, this parameter is conveniently chosen to be the initial radius R_0 instead of the φ_0, which is more stable and simpler to obtain, in particular in the thin wall limit[1]. While some completely numerical packages in the literature fail in the thin wall regime, our method computes the bounce and with similar speed in both thick and thin limits. Moreover, this approach solves the numerical instabilities when $\rho \to 0$ boundary $\rho \to \infty$ with its semi-analytical behavior.

As our benchmark, we present a linearly displaced quadratic potential defined as $V = \frac{\lambda}{8}(\varphi^2 - v^2)^2 + \epsilon(\frac{\varphi - v}{2v})$ with $\lambda = 1/4$ and $v = 1$, as shown in the top left panel of Fig. 2 in gray. Its resulting bounce action is on the bottom, computed with the polygonal method for different field point values and normalized to 400 points. The solid lines show the convergence of the action with respect to the number of segments N in $D = 4$ which goes below permille level accuracy with $\mathcal{O}(100)$ field segments. Each line corresponds to different ε that defines the differences in energy of the two minima, *i.e.* $\epsilon \propto |\tilde{V}_N - \tilde{V}_1|$. The inset shows the same for a smaller number of segments and the dotted lines show the comparison to other methods and tools. It includes CosmoTransition [18], AnyBubble [19], and shooting method. This approach was also tested in a model with the known exact bounce solution and in $D = 3$, where the convergences are similar.

Note that since the number of field points N is arbitrary, one can increase the number of segments until the actual potential is fully described. The exact solution of the bounce is provided when the number of segments goes to infinity $N \to \infty$. Nevertheless, few segments $\mathcal{O}(10)$ find a relevant precise action, comparable to other methods in the literature. Besides, the boundary conditions are solved analytically, which makes our method robust and relatively fast to compute the decay rate. In general, we found that the pre-factor contributes within $\mathcal{O}(1)$ percent to the decay rate, thereby extremely high precision of the bounce is unnecessary since it is overcome by the quantum and/or thermodynamic fluctuations of the bounce.

3.2. Extending polygonal bounce

In this section, we describe the inclusion of terms beyond linear order of the potential to the bounce through a linear perturbation around the

[1] As in [2], when the bounce φ is very close to the true vacuum $\tilde{\varphi}_1$, the solution is given by $\varphi(\rho) - \tilde{\varphi}_1 = 2(\varphi_0 - \tilde{\varphi}_1) I_{D/2-2}(m\rho)/m\rho$ where $m^2 \equiv V''(\tilde{\varphi}_1)$. Thereby, the initial condition $\varphi(R_{\rm in}) \equiv \varphi_0$ is exponentialy fine tuned, especially in the thin wall limit where $R_{\rm in} \gg 1/m$.

polygonal bounce. This procedure exploits the semi-analytical properties of the polygonal bounce to compute the corrections completely analytically. The inclusion of non-linear terms might describe the potential more suitably, as shown in the top left panel of figure 3 for $N = 7$ field points. In such cases it significantly enhances the converge of the action.

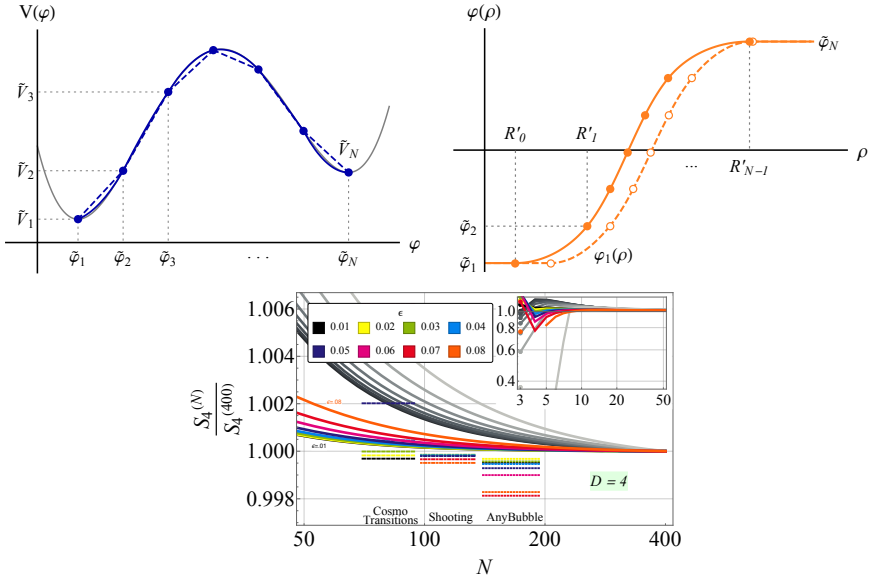

Fig. 3. (Color online) Top left: The polygonal potential with $N = 7$ field points in dashed black/blue and with the inclusion of non-linear terms in solid black/blue, circumscribed by the potential V in gray. Top right: The bounce field configuration of the polygonal potential on the left, PB dashed and extension PB solid. Bottom: The bounce action $S_D^{(N)}$ for different values of energy gaps between the false and true vacua, similar to figure 2, and computed for different field point values N normalized to $N = 400$ uniform segmentation in $D = 4$. The results are compared with other methods and polygonal bounce in gray.

To introduce this procedure, consider the polygonal bounce $\varphi = \varphi_{\rm PB}$ as an Ansatz field configuration to solve the equation of motion of a general potential V as

$$\ddot{\varphi}_{\rm PB} + \frac{D-1}{\rho}\dot{\varphi}_{\rm PB} - 8a = \delta {\rm d}V\left(\varphi_{\rm PB}(\rho)\right) , \tag{10}$$

where $\delta {\rm d}V(\rho)$ is defined as residual term that comes from the non-linear contributions of the potential and vanishes on the piece-wise linear potential. These contributions can be taken into account by the inclusion of a linear

expansion of the field $\varphi \to \varphi_{\rm PB} + \xi$ and Taylor series of the potential around the polygonal bounce $\varphi_{\rm PB}$ of equation (10)

$$\xi_s(\rho) \;=\; \nu_s + \frac{2}{D-2}\frac{\beta_s}{\rho^{D-2}} + \frac{4}{D}\alpha_s\rho^2 + \mathcal{I}_s(\rho)\,, \tag{11}$$

$$V \;=\; \tilde{V}_s - \tilde{V}_N + \partial\tilde{V}_s\,(\varphi_s - \tilde{\varphi}_s) + \frac{\partial^2\tilde{V}_s}{2}\,(\varphi_s - \tilde{\varphi}_s)^2 + \dots\,, \tag{12}$$

which implies

$$\mathcal{I}_s = \int_{\rho_0}^{\rho} \mathrm{d}y\, y^{1-D} \int_{\rho_1}^{y} \mathrm{d}x^{D-1}\partial^2\tilde{V}_s\,(\varphi_{\rm PB} - \tilde{\varphi}_s)\;, \tag{13}$$

where the constants $\partial V_s, \partial^2 V_s, \dots$ are determined by matching the values and (higher) derivatives of V, ρ_1, ρ_1. When N increases, the segmentation becomes arbitrarily dense and thus the terms beyond the linear one in (12) become progressively negligible.

The boundary conditions are the same as for the polygonal bounce, $\varphi_s(R_s) = \varphi_{s+1}(R_{s+1}) = \tilde{\varphi}_s$ and $\dot{\varphi}_s(R_s) = \dot{\varphi}_{s+1}(R_{s+1})$, where they can be solved completely analytically after a linear expansion around the radii from the polygonal solution as

$$R_s \to R_s\,(1 + r_s)\;, \qquad r_s \ll 1 \tag{14}$$

which makes this contributions fast and convenient to implement. The actions from the polygonal bounce and its extension are displayed in the bottom panel of figure 3 as gray (top) and color (bottom) solid lines respectively. In this case, the convergence is up to three times faster than the pure polygonal bounce.

3.3. Pre-factor: loop correction

The properties of the polygonal bounce solution can be exploited to compute the pre-factor of the decay rate Eq. (2) semi-analytically. This loop correction was originally derived in [3] and studied in different aspects that include numerical methods in $D = 3$ [20, 21] and $D = 4$ [22, 23], precision calculations in presence of gauge interactions [24], scale-invariant instantons and extended gauge theories [25]. Nevertheless, not many explicit analytical results on the pre-factor are available with a notable exception of the thin wall limit [26].

The total decay rate at one loop in $D = 4$ is

$$\Gamma = \left(\frac{S_4}{2\pi}\right)^2 \left|\frac{\det'(-\partial^2 + V''(\varphi(\rho)))}{\det(-\partial^2 + V''(\varphi_-))}\right|^{-1/2} \mathrm{e}^{-S_4 - \delta_4}\,, \tag{15}$$

where S_4 is the semi-classical action computed from the bounce solution $\varphi(\rho)$ and $\det'$ is the determinant of the fluctuation operator $\mathcal{O}$, *i.e.* the second variation of the action. Finally, δ_4 is the perturbative one-loop counterterm of the action that absorbs the renormalization infinities.

As in the work of Dunne [23], the fluctuation operator is decomposed in a multipole expansion due to the $O(4)$ symmetry of the semi-classical solution

$$\mathcal{O}_l = -\frac{\mathrm{d}^2}{\mathrm{d}\rho^2} - \frac{3}{\rho}\frac{\mathrm{d}}{\mathrm{d}\rho} + \frac{l(l+1)}{\rho^2} + V''(\rho)\,. \tag{16}$$

Here, it is convenient to use the Gel'fand–Yaglom theorem [27] that relates the ratio of determinants to the value of the ratio of eigenfunctions $\psi_l(\rho)$ of $\mathcal{O}_l$ evaluated at infinite Euclidean time

$$\frac{\det \mathcal{O}_l}{\det \mathcal{O}_l^{\text{free}}} = \mathcal{R}_l(\rho=\infty)^{(l+1)^2}\,, \qquad \mathcal{R}_l(\rho) = \frac{\psi_l(\rho)}{\psi_l^{\text{free}}(\rho)}\,. \tag{17}$$

One can consistently compute the eigenfunctions of Eq. (16) on the extending polygonal bounce solution, *i.e.*, Eqs. (8) and (11), where $V'' = \partial^2\tilde{V}$ is constant introduced in (12). With this simplification, the solutions of the fluctuation operator can be obtained in a closed form for each segment and joined to get a new semi-analytical solution of the pre-factor. This approach can be expanded to an arbitrary number of space-time dimensions and help us understand the pre-factor in multiple scalar field potentials.

3.4. Multi-field polygonal bounce

In this section, we describe the generalization of the polygonal bounce approach to an arbitrary number of scalar fields. We start with an Ansatz $\bar{\varphi}_{is}$ obtained from an chosen set of points in field space $\tilde{\varphi}_{is}$ that connects the two minima, for instance a straight line as shown in the top left panel of Fig. 4; and its corresponding longitudinal polygonal bounce is in the top right, where i is the field index $i = 1, \ldots, n_f$ and $s = 1, \ldots, N-1$ for each segment.

Similar to Section 3.2, we improve the Ansatz by a linear expansion around the initial estimate $\varphi_{is}(\rho) = \bar{\varphi}_{is} + \zeta_{is}$ in the equation of motions

$$\underbrace{\ddot{\bar{\varphi}}_{is} + \frac{D-1}{\rho}\dot{\bar{\varphi}}_{is}}_{8\bar{a}_{is}} + \underbrace{\ddot{\zeta}_{is} + \frac{D-1}{\rho}\dot{\zeta}_{is}}_{8a_{is}} = \frac{\mathrm{d}V}{\mathrm{d}\varphi_i}\left(\bar{\varphi}+\zeta\right)\,, \tag{18}$$

together with a linear Taylor expansion of the potential around the initial field points $\mathrm{d}_i\tilde{V}_s = \mathrm{d}_i V(R_s)$, as

$$\frac{\mathrm{d}V}{\mathrm{d}\varphi_i} \simeq \frac{\mathrm{d}_i\tilde{V}_s + \mathrm{d}_i\tilde{V}_{s+1} + \mathrm{d}^2_{ij}\tilde{V}_s\tilde{\zeta}_{js} + \mathrm{d}^2_{ij}\tilde{V}_{s+1}\tilde{\zeta}_{js+1}}{2}\,, \tag{19}$$

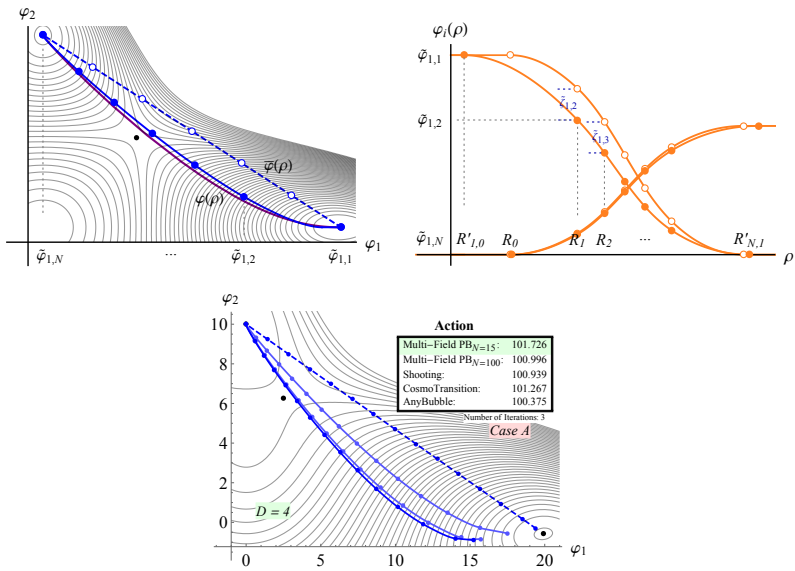

Fig. 4. Top left: Path in field space with the initial straight dashed line Ansatz $\bar{\varphi}$ with empty circles and the first iteration of the PB solution in solid black/blue and full circles; the result from shooting is shown in black/purple. Top right: Iterations of the bounce field configuration for $\varphi_1(\rho)$. Bottom: Multi-field polygonal solution in $D = 4$ with $N = 15$ segmentation points. The starting Ansatz is the straight dashed line connecting the two minima, shown as black dots, together with the saddle point. The solid lines are subsequent iterations that converge to the final path that solves the bounce equations. Insets show the action compared to other approaches.

where the gradient in (19) has to be expanded up to the second derivative of the potential since it contains information of the interaction of the fields and describes curved paths in field space. In contrast to the single field case, the idea is to look for a set of new field points $\tilde{\varphi}_{is} + \tilde{\zeta}_{is}$ that satisfies the boundary conditions $\varphi_{is}(R_s) = \varphi_{is+1}(R_s)$ and $\varphi_{is}(R_i) = \varphi_{is+1}$ and solves equations (18) on the linear expansion (19) as shown in figure 4. This is realized iteratively and it converges once the path in field space does not change anymore, *i.e.* $\tilde{\zeta}_{is} \simeq 0$. The multi-field bounce solution for a constant derivative of the potential $\mathrm{d}V/\mathrm{d}\varphi_i$ is again polygonal type

$$\zeta_{is}(\rho) = v_{is} + \frac{2}{D-2}\frac{b_{is}}{\rho^{D-2}} + \frac{4}{D}a_{is}\rho^2\,. \tag{20}$$

Here, a_{is} corresponds to the leading constant expansion of the gradient of the potential around some deformed path, defined by $\tilde{\varphi}_{is} + \tilde{\zeta}_{is}$. Since part of

the solution is known in a closed form, it lets us to transform the boundary conditions into a system of linear equations, which are solvable efficiently. Thereby, the multi-field polygonal bounce is computed fast and increases linearly with the number of fields and field points. As an example, we consider a simple two field potential $V(\varphi_i) = \sum_{i=1}^{2}(-\mu_i^2\varphi_i^2 + \lambda_i^2\varphi_i^4) + \lambda_{12}\varphi_1^2\varphi_2^2 + \tilde{\mu}^3\varphi_2$ with μ_1^2, $\mu_1^2 = 100$, $\lambda_1 = 0.1$, $\lambda_2 = .3$, $\lambda_{12} = 2$ and $\tilde{\mu}^3$ as shown in Fig. 4. From the insets, the PB action is quite precise even with $N = 15$ and reaches roughly permille precision with $N = 100$.

3.5. Package: FindBounce

The creation of a robust and efficient package for the evaluation of the lifetime of a false vacuum is in progress [17]. It is based on the polygonal bounce idea, which grows linearly with the number of fields and field points, and computes the bounce transition in quantum and thermal multi-field theories up to the desired precision at a competitive speed. The package is called FindBounce, it is simple to use with the native Mathematica look and feel. It is easy to install and comes with detailed documentation and physical examples. It computes the bounce action in a non-trivial 20 field potential in 3 seconds and within 1% accuracy.

4. Conclusions and outlook

We developed a semi-analytical, simple and efficient approach to compute the false vacuum decay rate of potentials with any number of fields up to the desired precision at zero and finite temperature. Besides, it provides an analytical insight into the pre-factor and the multi-field phase transitions of the vacuum. This approach is also useful to study potentials with multiple minima and resonant tunneling effects [28]. The convergence is linear concerning the number of fields and segments, which make it fast and robust. Since part of the solution is known in polygonal bounce, the bounce is computed by finding a more stable initial condition that allows us to compute in very thin wall regimens. We are releasing a Mathematica package that computes the bounce action at competitive speed: around 3 seconds for 20 fields potential and within 1% accuracy.

REFERENCES

[1] I.Y. Kobzarev, L.B. Okun, M.B. Voloshin, *Sov. J. Nucl. Phys.* **20**, 644 (1975) [*Yad. Fiz.* **20**, 1229 (1974)].

[2] S.R. Coleman, *Phys. Rev. D* **15**, 2929 (1977) [*Erratum ibid.* **16**, 1248 (1977)].

[3] C.G. Callan, Jr., S.R. Coleman, *Phys. Rev. D* **16**, 1762 (1977).

[4] S.R. Coleman, *Aspects of Symmetry: Selected Erice Lectures*, Cambridge University Press, 1985, DOI:10.1017/CBO9780511565045.

[5] I. Affleck, *Phys. Rev. Lett.* **46**, 388 (1981).

[6] A.D. Linde, *Phys. Lett. B* **70**, 306 (1977).

[7] A.D. Linde, *Phys. Lett. B* **100**, 37 (1981).

[8] A.D. Linde, *Nucl. Phys. B* **216**, 421 (1983) [*Erratum ibid.* **223**, 544 (1983)].

[9] M. Trodden, *Rev. Mod. Phys.* **71**, 1463 (1999) [arXiv:hep-ph/9803479].

[10] J.M. Cline, arXiv:hep-ph/0609145.

[11] J.S. Langer, *Ann. Phys.* **41**, 108 (1967) [*Ann. Phys.* **281**, 941 (2000)].

[12] J.S. Langer, *Ann. Phys.* **54**, 258 (1969).

[13] M.J. Duncan, L.G. Jensen, *Phys. Lett. B* **291**, 109 (1992).

[14] S.R. Coleman, V. Glaser, A. Martin, *Commun. Math. Phys.* **58**, 211 (1978).

[15] K. Blum *et al.*, *J. High Energy Phys.* **1705**, 109 (2017) [*Erratum ibid.* **1706**, 060 (2017)] [arXiv:1611.04570 [hep-th]].

[16] V. Guada, A. Maiezza, M. Nemevšek, *Phys. Rev. D* **99**, 056020 (2019) [arXiv:1803.02227 [hep-th]].

[17] V. Guada, M. Nemevšek, M. Pintar, work in progress.

[18] C.L. Wainwright, *Comput. Phys. Commun.* **183**, 2006 (2012) [arXiv:1109.4189 [hep-ph]].

[19] A. Masoumi, K.D. Olum, B. Shlaer, *J. Cosmol. Astropart. Phys.* **1701**, 051 (2017) [arXiv:1610.06594 [gr-qc]].

[20] A. Strumia, N. Tetradis, *Nucl. Phys. B* **542**, 719 (1999) [arXiv:hep-ph/9806453].

[21] G. Münster, S. Rotsch, *Eur. Phys. J. C* **12**, 161 (2000) [arXiv:cond-mat/9908246].

[22] J. Baacke, G. Lavrelashvili, *Phys. Rev. D* **69**, 025009 (2004) [arXiv:hep-th/0307202].

[23] G.V. Dunne, H. Min, *Phys. Rev. D* **72**, 125004 (2005) [arXiv:hep-th/0511156].

[24] A. Andreassen, D. Farhi, W. Frost, M.D. Schwartz, *Phys. Rev. D* **95**, 085011 (2017) [arXiv:1604.06090 [hep-th]]; A. Andreassen, W. Frost, M.D. Schwartz, *Phys. Rev. D* **97**, 056006 (2018) [arXiv:1707.08124 [hep-ph]].

[25] S. Chigusa, T. Moroi, Y. Shoji, *Phys. Rev. D* **97**, 116012 (2018) [arXiv:1803.03902 [hep-ph]].

[26] R.V. Konoplich, S.G. Rubin, *Yad. Fiz.* **42**, 1282 (1985); R.V. Konoplich, *Theor. Math. Phys.* **73**, 1286 (1987) [*Teor. Mat. Fiz.* **73**, 379 (1987)].

[27] I.M. Gel'fand, A.M. Yaglom, *J. Math. Phys.* **1**, 48 (1960).

[28] V. Guada, M. Nemevšek, L. Ubaldi, work in progress.